



## APPLICATION OF GOOD CFD SIMULATION PRACTICES TO S814 AIRFOIL PROFILE

**Graziela Gomes de Magalhães Melo**  
**Lucas Amaro de Oliveira**  
**Alex Maurício Araújo**  
**Aigbokhan Isaiah Asibor**  
**Armando Lúcio Ramos de Medeiros**  
**Oyama Douglas Queiroz de Oliveira Filho**  
**Rafael Luz Espindola**  
**Héric César Martins Machado**

Federal University of Pernambuco, Department of Mechanical Engineering, Prof. Moraes Rêgo Av., 1235 - Cidade Universitária, Recife - PE - Brazil - Zip Code: 50670-901 - Phone: +55 81 2126-8000. e-mails: [melo.graziela@gmail.com](mailto:melo.graziela@gmail.com); [eng.amaro@yahoo.com](mailto:eng.amaro@yahoo.com); [ama@ufpe.br](mailto:ama@ufpe.br); [issy\\_asibor@yahoo.com](mailto:issy_asibor@yahoo.com); [armandolucio@bol.com.br](mailto:armandolucio@bol.com.br); [oyamadouglas@gmail.com](mailto:oyamadouglas@gmail.com); [rafael\\_luzes@hotmail.com](mailto:rafael_luzes@hotmail.com); [heric.cesar@yahoo.com.br](mailto:heric.cesar@yahoo.com.br).

**Philippe Jaouen**  
**Ricardo E. Noguera**

Arts et Métiers Paristech, Boulevard de l'Hôpital, 151, Zipcode : 75013, Paris - France.  
e-mails: [philippe.jaouen@gadz.org](mailto:philippe.jaouen@gadz.org); [ricardo.noguera@ensam.eu](mailto:ricardo.noguera@ensam.eu).

**Abstract.** *Good CFD simulation practices are currently considered as essential requirements to approach reality in studying the behavior of many fluid flows. For classical airfoil profiles, whose information is widely available in literature, a good simulation practice should result in overall values of drag and lift forces consistent with experimental data obtained in wind tunnel. Otherwise, some key factors to the simulation success such as the size of the computational domain, the number of nodes in the mesh, boundary conditions and turbulence model should be revised. During the testing process of these multiple factors, best simulation practices can be adopted not only for guidance but also to accelerate the delivery of consistent results in the simulation process. This article aims to present the results obtained with the procedure in simulating the behavior of S814 airfoil with CFD FLUENT®, varying those factors, except the turbulence model, until obtain values consistent with lift experimental data.*

**Keywords:** *lift, drag, mesh, computational domain, boundary conditions.*

### 1. INTRODUCTION

CFD simulations are now widely used in various fields of engineering. In the area of wind power its application has intensified in recent years, both in the aerodynamic design of rotors and in the evaluation of wind resource. This article aims to identify the main difficulties in the application of CFD and propose best practices- a procedure to guide and accelerate its application in problems in the field of wind energy. In general, using CFD to solve a real practical problem, the main difficulty consists in the adoption of various parameters for constructing the computational model. This paper demonstrates that the results of CFD simulations will be more reliable if the best practices are adopted for the parameters involved, such as size and type of the computational domain, mesh type and specification of boundary conditions.

A more appropriate method for airfoil CFD simulation was not found in reviewed literature. Therefore, this study was based on the analysis of various methods applied directly to the problem such as in Singha et al. (2010), Hills (2005), Ribeiro (2011), Knoppa et al. (2009), and a test methodology has been proposed in order to better organize and optimize the simulation procedure. For applying the proposed methodology, was chosen S814 airfoil which is dedicated specifically for wind turbine blades from 20 to 40 m at the root region (Buhl, 2012).

In general, experiments in wind tunnels are used for validating CFD simulations, however for this work, the opposite way was adopted - using the experimental data from Somers (1997), this work tried to obtain the control variable value with the use of simulation best practices. The criteria for assessing the quality of the simulation was approximating the value of the lift coefficient with an angle of attack of 10°, which has an experimental value of 1.32 (Somers, 1997).

### 2. FEATURES OF EXPERIMENT

#### 2.1 Wind tunnel experiments

In the work realized by Somers (1997), the wind tunnel experiment occurred at *Delft University of Technology Low Speed Laboratory* and the dimensions of the tunnel section are: 2.6 x 1.248 x 1.25 m (Delf University of Technology,

2013). Once an increase in the roughness causes a decrease in the lift coefficient, especially on the leading edge (Huang *et al.*, 2011) the S814 profile has been developed with the aim of presenting insensitivity to this increased roughness. In addition, the S814 was designed with a thickness of 24% in relation to the chord to meet the characteristics of the blade root region.

The wind tunnel experiment consisted of two goals. The first was to demonstrate the insensitivity of the airfoil according to the change in roughness near the leading edge, since there is usually constant accumulation of debris in this area. The second goal showed that in a lift coefficient range of 0.6 to 1.2, low drag coefficient values are obtained.

To test the insensitivity of the airfoil, the first step was to test it with a smooth surface. In the second step, sand strips were added in order to increase turbulence and cause vortex formation and therefore comparing the results of the first and second steps to confirm the surface roughness insensitivity of the S814. In order to test the best practices in the case of CFD simulations, the condition of free transition was chosen, ie, the regime is turbulent, but the increase of this turbulence is not forced on the leading edge.

In a nutshell, among the various scenarios tested in Somers (1997), free transition, better lift (10°), Reynolds number  $1.5 \times 10^6$  and Mach number 0.10, were chosen for the implementation of good practices. For this Reynolds number and the condition of free transition, the maximum lift value was 1.32 which according to Somers (1997) exceeds by 2%, the theoretically expected value.

**1.1 Type of airfoil**

The airfoil S814 (Fig.1), of which dimensions are available at the *National Wind Technology Center website* was developed for the root of horizontal wind turbine blade and with a thickness greater than the traditional airfoils. Despite the higher concentration of the roughness on the blade tip, yet there is an accumulation of debris at the root, mainly on the leading (Sagol *et al.*, 2012). This airfoil presents a complex geometry and its 24% thickness contributes to a maximum lift coefficient, insensitive to roughness on the leading edge and with a low drag profile. Furthermore, Somers (1997) showed that the maximum relation lift/drag occurs simultaneously for the maximum lift coefficient.

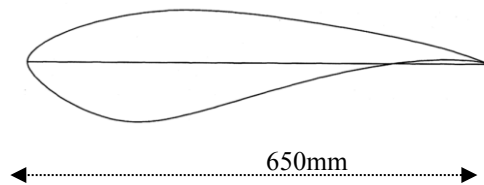


Figure1. Aerofólio S814

**3. GOVERNING EQUATIONS AND k-ω SST TURBULENCE MODEL**

In computational fluid dynamics, differential equations of flow are used: steady Navier-Stokes (Eq.1) and the continuity equation (Eq.2). Equations 1 and 2 are valid for incompressible, viscous and laminar flow.

$$(\vec{\nabla} \cdot \vec{v}) - \frac{1}{\rho} \nabla^2 p = 0 \tag{1}$$

$$\vec{\nabla} \cdot \vec{v} = 0 \tag{2}$$

Where  $V$  is the speed,  $\rho$  is the specific mass,  $\nu$  kinematic viscosity and  $p$  the modified pressure.

For turbulent flows, Eq. 1 cannot be used without a turbulence model. The turbulence models are approximations resulting from experiments which contain several empirical constants associated with direct numerical simulations.

With the turbulence model, the specific Reynolds stress tensor is added (Eq.3) to the general equation (Eq. 4), which becomes known as the Reynolds-averaged Navier-Stokes (RANS).

$$\vec{\nabla} \cdot \vec{v} - \frac{1}{\rho} \nabla^2 p - \vec{\tau}_{i, turbulent} = 0 \tag{3}$$

$$(\vec{\nabla} \cdot \vec{v}) - \frac{1}{\rho} \nabla^2 p - \vec{\tau}_{i, turbulent} = 0 \tag{4}$$

These tensor (Eq. 4) are modeled according to several turbulence models which add new equations that are solved simultaneously with Eqs 2, 3 and 4 (Çengel and Cimbala, 2007).

Turbulence models often do not represent well situations with flow separation, reattachment and / or transience of the system on a large scale (Çengel and Cimbala, 2007). The model used in this work was the  $k-\omega$  SST. In comparative tests with other turbulence models, for example, from the work by Knoppa et al. (2009) a test between the  $k-\omega$  SST models and SA models was performed (Edwards and Chandra, 1996) and the  $k-\omega$  SST model best predicted the detachment of the boundary layer. According to Menter (1993), the turbulence model  $k-\omega$  SST is used instead of the standard  $k-\omega$  since the former is known to give superior results for flow with separation in the boundary layer. The equations to be added in Eq. 4 are (SAS IP, 2011):

$$\frac{d}{dt} \left( \rho u_i \right) = - \left( \frac{\partial}{\partial x_j} \right) \tilde{\tau}_{ij} \quad (5)$$

$$\frac{d}{dt} \left( \rho \omega \right) = - \left( \frac{\partial}{\partial x_j} \right) \tilde{\tau}_{\omega j} + \omega_{\text{gen}} - \omega_{\text{diss}} + \omega_{\text{cross}} + e_{\omega} \quad (6)$$

Where  $k$  represents turbulent kinetic energy;  $\omega$  specific dissipation rate;  $\tilde{\tau}$  represents the generation of kinetic energy due to the average speed;  $\omega_{\text{gen}}$  represents the generation of  $\omega$ ;  $\tilde{\tau}_{ij}$  and  $\tilde{\tau}_{\omega j}$  represent the effective diffusivity of  $k$  and  $\omega$  respectively;  $\omega_{\text{diss}}$  and  $\omega_{\text{cross}}$  represent the dissipation of  $k$  and  $\omega$  due to turbulence;  $\omega_{\text{cross}}$  represent the cross-term diffusion;  $e_{\omega}$  are sources defined by the user.

#### 4. GOOD PRACTICES

Most of the problems involving airfoil simulation in literature is resolved with bidimensional models, since less computational time and lower number of cells are required, consequently. Some models are also developed with a small span, which thus leads to a three-dimensional problem, even with a reduction of one of its dimensions. This way, the computational time of the problem decreases (Yuguang *et al*, 2010).

The first step to be taken in relation to the simulation is knowing what type of computational domain is going to be used to decrease the wall effect or the formation of sharp edges. Furthermore, the size should be sufficient in order to be represented the simulation if there is a formation of wakes.

The second step is the selection and treatment of mesh, which depending on the type and how refined it is, its creation exceeds the convergence time of the calculations. For selecting the mesh type, i.e., the choice between a structured mesh or non-structured, considerations need to be made about the geometry of the problem and how refined the mesh must be. Unstructured meshes are usually used for complex geometries and for a high level of processing and memory.

According to Çengel and Cimbala (2007), the structured meshes work best when compared to non-structured mesh because they ensure good visualization and calculation of forces. The structured mesh relies heavily on the behavior of the flow in the boundary layer, where the variables change rapidly in the direction normal to the flow, since they allow a greater refinement for the same number of cells that would be thinner and strongly compact. In addition, the greater the refinement, less the discretization error and the more faithful will be the adopted mathematical models to the results. According to Germer (2009), the application of mesh refinement is justified when the geometry presents discontinuities or large gradients of some property of interest.

With respect to the distribution of the mesh cells, for Schneider (2007), the use of domain division is more widespread and the resolution of the simulations with the use of multiblocks in irregular or complex geometries. For a regular domain, the unstructured meshes are not advisable, because the computational time to resolve the problem increases.

Besides the refinement of the boundary layer mesh, a good practice to be used in the simulations is the directional refining, i.e., in the boundary layer, in its leading edge and at the trailing edge, where could be vortex formation and/or formation of wakes. A counterpart in refining the mesh is the calculation time. The more refined the mesh, the more the simulation time is required by the computer for the results to converge. Therefore a study of mesh independence is essential to avoid unnecessary simulation time.

In the processing step, it is of great advantage to observe the graphical behavior of the control variable and the residue equations to monitor the results of the iterations. If the residues are not approaching zero or the control variable is not converging to a constant value, the simulation can be stopped and an analysis of the parameters can be remade. Apart from re-examining the parameters adopted, the CFD software allows to observe the velocity field vector behavior in order to visually identify anomalies in the flow possibly caused by errors in the mesh, since this is the most critical factor in CFD simulations.

#### 5. METHODOLOGY

At first, were chosen the boundary conditions related to the type of software. In the initial simulation conditions, an analysis of what best initial velocity could be used. In section 5.2, an analysis of the domain size was developed. Then,

in section 5.3, a study of the choice of structured and unstructured mesh was carried out and independence test was also performed.

The software used was ANSYS Fluent ® and the algorithm was SIMPLE. A bi-dimensional, incompressible and permanent air flow was considered in the simulations. For the control variable of the simulations relations between the lift coefficient values for various angles of attack and the experimental values were used .

### 5.1 Boundary conditions

For each edge of the domain one boundary peripheral condition is specified. According to Fig. 4, for the airfoil and the top and bottom edges the *wall* condition was determined; the *velocity inlet* condition was determined for the inlet edge, and the *outlet pressure* for outlet edge. In the *wall* boundary conditions, including the airfoil, the *non slip* condition was determined i.e. the velocity of the fluid in contact with the airfoil is the same as the airfoil. In this case, the speed tangential component in a fixed wall equals zero (Çengel and Cimbala, 2007).

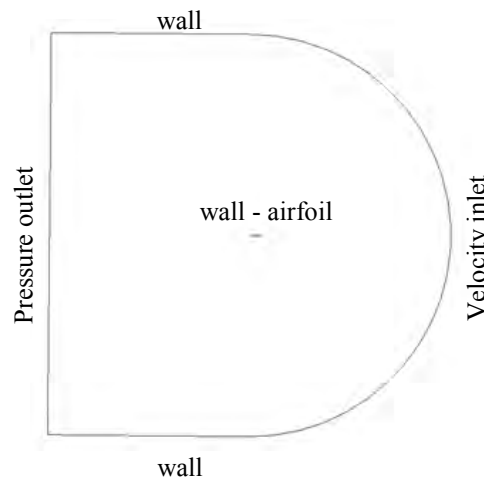


Figure 4. Boundary conditions used for the software Ansys Fluent®.

Air was considered to be the fluid, pressure of 1 atm and isothermal flow at 298 K, i.e. the energy equation is not solved. Since the information obtained from Somers (1997) was used, for a Reynolds equal to  $1.5 \times 10^6$ , the inlet velocity was calculated from Eq. 7.

$$e = \frac{c}{Re} \quad (7)$$

Where  $c$  is the chord size of the airfoil, 0.65m;  $\nu$  is the kinematic viscosity  $1.562 \times 10^{-5} \text{ m}^2/\text{s}$  at 1 atm and 298 K;  $Re$  the Reynolds number  $1.5 \times 10^6$ . This way, from this data the speed is approximately 36 m/s.

In Janiszewska *et al.*(1996), it was shown that the lift coefficient does not vary significantly for the number of Reynolds from  $0.75 \times 10^6$  to  $1.5 \times 10^6$ . Simulations with the speeds 9, 24 and 36 m/s were performed with the aim of simulating this behavior, where the corresponding Reynolds according to Eq.7 are  $3.7 \times 10^5$ ;  $1.0 \times 10^6$ ;  $1.5 \times 10^6$  respectively.

### 5.2 Computational domain

Two types of domain are commonly used. The O-mesh domain (Ribeiro *et al.*, 2011) has circular shape and the C-mesh domain has a semicircle at the entrance and a coupled rectangle, which allows for a good simulation of the wake. Therefore, the latter was chosen for all simulations.

A size large enough for the domain is essential so as not to interfere with the flow field. In the work presented by Hills (2005) the C-mesh domain size compared to the chord ( $c$ ) was  $32.5c \times 25c$ . While in this study, relating the size of the domain with the S814 chord, the size of the area was approximately  $40c \times 19c$ , since the experiment was carried out by testing the dimensions of the wind tunnel.

Simulations were performed with two fields with the C-mesh format (Fig. 5), but with different dimensions. Domain I has the same dimensions as the wind tunnel test section:  $a = 2.6 \text{ m}$  and  $b = 1.25 \text{ m}$  and domain II, the dimensions  $a = 26 \text{ m}$  and  $b = 12.5 \text{ m}$ . And the airfoil chord used in both domains of the experiment was the same and equal to 0.65 m.

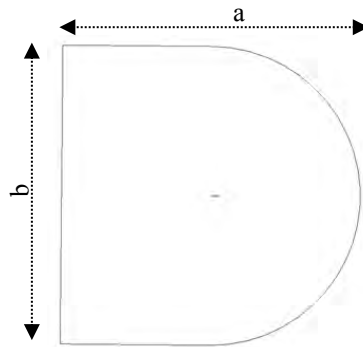


Figure 5. C-mesh domain size.

### 5.3 Mesh

Although having already seen in the reviewed literature that the mesh structured is the best option for the simulation of airfoils, simulations were performed for structured and unstructured meshes. The domain II was used in the two mesh types, and number of nodes for structured and unstructured mesh was respectively 506.674 and 643.982.

The mesh independence consisted of increasing refinement of best mesh type tested and thus verifies the sensitivity of the control variable. If it changes little with successive refinement, then it was reached the optimal number of nodes and the increase of its refinement will cause an unnecessary calculation time.

#### 5.3.1 Stagnation point

Figure 6 shows a part of the semicircle domain refinement corresponding to the input flow. As the mesh in the semicircle is already refined for any flow direction, the directional refinement for each angle does not need be performed. Moreover, the stagnation point of the flow on the trailing edge is best discretized.

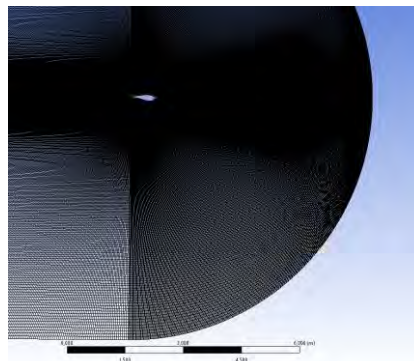


Figure 6. Refinement of the semicircle at the inlet flow of the domain.

#### 5.3.2 Boundary layer and trailing edge

The behavior of the boundary layer is complex but it can be said that it depends on the Reynolds number at which the airfoil is subjected, to the aerodynamic airfoil, the Mach number and also the rough surface (Hansen, 2008). Thus, special treatment is needed in the boundary layer of the airfoil for purposes of simulating the wind flow.

From both examples in Fig.8, further refinement is seen in the immediate airfoil contour. Moreover, beyond this boundary, there is a perceived difference in the refinement of the cells between the two examples. On the left, there is a gradual increase in the boundary layer cells and beyond, and to the right there is an abrupt refinement and the mesh is overly refined, increasing the computation time unnecessarily. According to Çengel and Cimbala (2007), rapid changes in the cell size can lead to convergence or numerical difficulties in the CFD code.

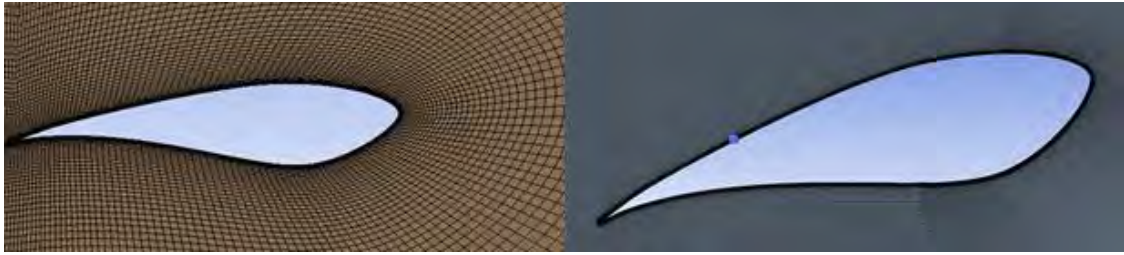


Figure 8. Mesh with progression on the left and unnecessarily refined mesh on the right.

### 5.3.3 Refinement at the wake region

Besides the greater refinement in the semicircle, another key point is the possible formation of wake. This way, after the trailing edge, it is observed in Fig. 9 that the refinement is being extended until the end of the computational domain.



Figure 9. Refinement in the semicircle and, after the trailing edge, refinement until the end of the computational domain.

Since the angle of attack is high and the regime is turbulent, there is a high chance of wake formation in this region. If after the simulation, this formation does not occur visually, refinement can be decreased and the calculation time would be lower, converging towards the same result.

## 6. RESULTS AND DISCUSSIONS

Table 1 presents a summary of the performed simulations.

Table 1. Simulation scenarios.

N°	Domain		Mesh	Turbulence Model	Angle of Attack	Inlet Velocity (m/s)
	Type	Size				
1	C-mesh	4cx1.9c	Structured	k- $\omega$ T	0°; 2°; 5°; 6.3°; 10°	36
2	C-mesh	40cx19c	Structured	k- $\omega$ T	0°; 2°; 5°; 6.3°; 10°	36
3	C-mesh	40cx19c	Structured	k- $\omega$ T	0°; 2°; 5°; 6.3°; 10°; 15°	36
4	C-mesh	40cx19c	Unstructured	k- $\omega$ T	0°; 2°; 5°; 6.3°; 10°; 15°	36
5	C-mesh	40cx19c	Structured	k- $\omega$ T	0°; 5°; 10°; 15°	9; 24 and 36

### 6.1 Visualization of the results

Once the simulation was performed, there is the post-processing step in which a visual analysis of the flow field is performed. In Fig.10, vectors of different colors representing their speeds are perceived, according to the scale. In Fig. 10 two items are worth mentioning: the stagnation point on the leading edge, where the flow is split into intrados and

extrados, and the detachment at the trailing edge which is better detailed in Fig. 11, where the return of flow is noted at the extreme of the trailing edge caused by the adverse pressure gradient. The vortex center caused by this return can also be seen. Only the formation of vortex is seen and not its propagation, since the simulations were performed in a steady state.

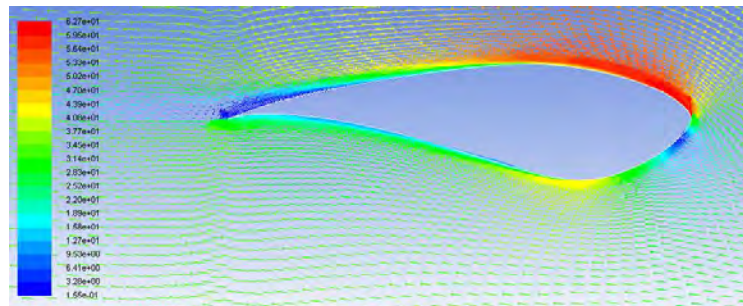


Figure 10. Post-processing and analysis of the velocity vectors.

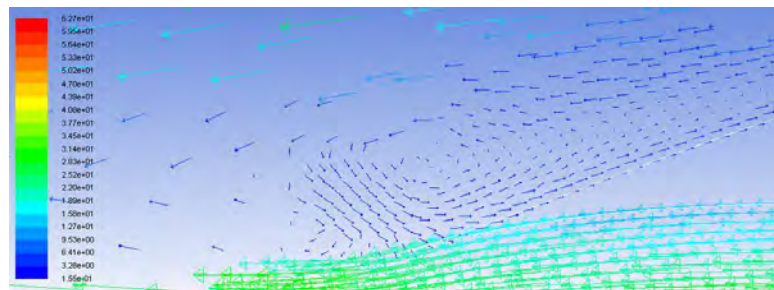


Figure 11. Detail of the bubble movement on the trailing edge.

The viscous air flow effects are important close to the airfoil region and, outside the boundary layer and vortex region, the flow behaves as a non-viscous fluid. Thus, the mesh must be properly refined in the region near the airfoil so that quantitative flow problems do not arise and the simulation flow approaches reality. In Fig. 12, there is a counterexample on the left of a good practice with respect to refinement, while the image on the right shows the inconsistency of the velocity vectors caused by this bad refinement.

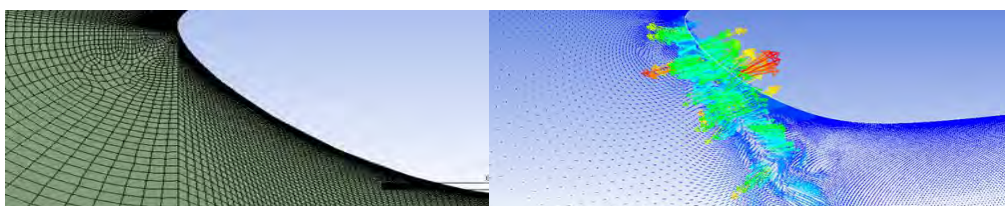


Figure 12. Counterexample of good practice in the boundary layer refinement which causes inconsistency in the speeds at the stagnation region.

## 6.2 Analysis of the domain size

The optimum size of the computational domain, as shown in item 5.2, should be that in which the wall effect does not interfere with the control variable and it should be possible to view a reliable flow. The result of the two domains tested with the scenarios n° 1 and n° 2 shown in Tab. 1 is shown in Fig. 13 where the graph relates the relative error (Eq. 7) with the angle of attack.

$$\frac{l - l_e}{l_e} \quad (7)$$

Where  $l$  is the lift coefficient value of the simulation and  $l_e$  the lift coefficient of the wind tunnel experiment.

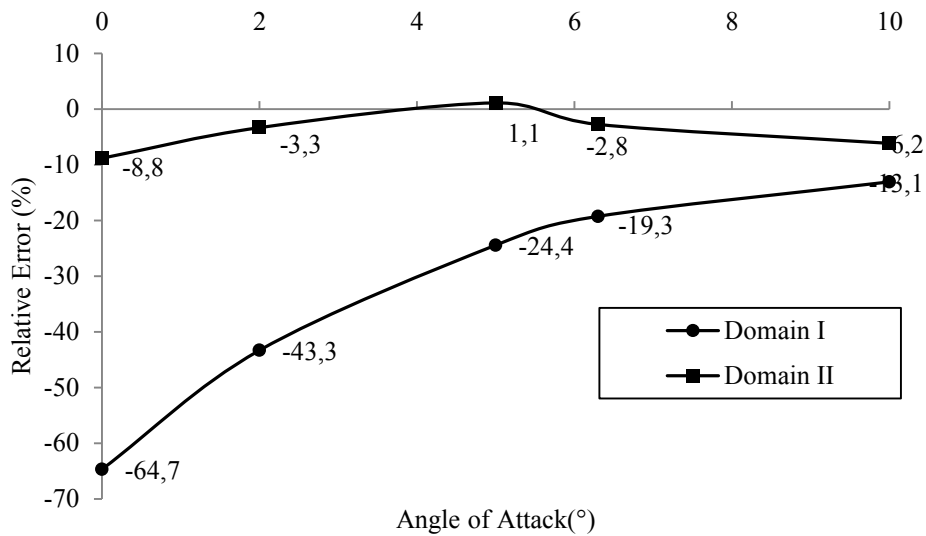


Figure 13. Graph of simulation errors using the domain I and II.

According to the behavior shown in Fig. 13, the domain I ( $4c \times 1.9c$ ) failed to produce a satisfactory result while domain II ( $40c \times 19c$ ) proved to be adequate.

### 6.3 Meshes

Using scenarios n° 3 and n° 4 of Tab.1, a comparison was made on the structured and unstructured mesh where the number of resultant nodes was 506.674 and 643.982 respectively. Figure 14 shows the lift coefficient values as a function of the angle of attack for both mesh types and the wind tunnel experiment.

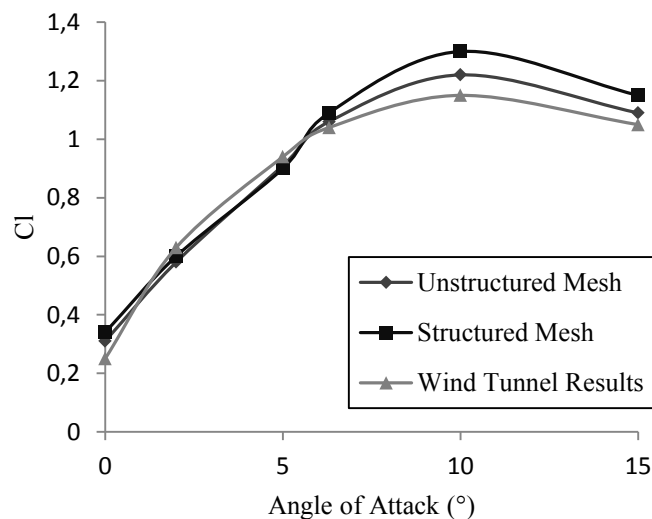


Figure 14. Comparison between the meshes and the wind tunnel experiment.

The result presented by the structured mesh is: for the angle of attack of  $10^\circ$ , the lift coefficient of 1.217 and this is closer to the value of the wind tunnel experiment (1.32). Having a structured mesh as a best practice in simulating this airfoil, independence test was made by carrying out refinement with various multiplicative factors, as seen in Tab.2. In this table it can be seen that as from 506.674 elements, the Cl result does not vary significantly with the refinement of 1.5, making refinement unnecessary as from this case.

Table 2. Refinement of the mesh

Multiplicative refinement factor with respect to the previous mesh		2	2.7	1.5	1.5	1.5	1.5
Number of nodes	56,812	120,000	326,782	506,674	798,634	1,242,812	1,890,296
Cl value	0.980	1.140	1.190	1.217	1.220	1.221	1.221

#### 6.4 Velocities

For the S814 profile and varying only the Reynolds number ( $0.75 \times 10^6$  a  $1.5 \times 10^6$ ), this does not significantly influence the lift coefficient with respect to the angle of attack as shown in item 5.1. To demonstrate the behavior of the airfoil shown in Fig. 15, simulations were performed according to scenario n° 5 from Tab.1, shown in Fig. 16, which proved the work done by Janiszewska et al. (1996).

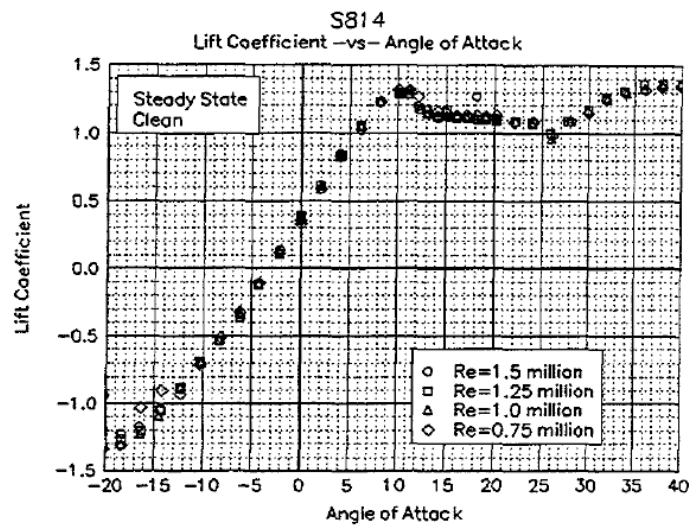
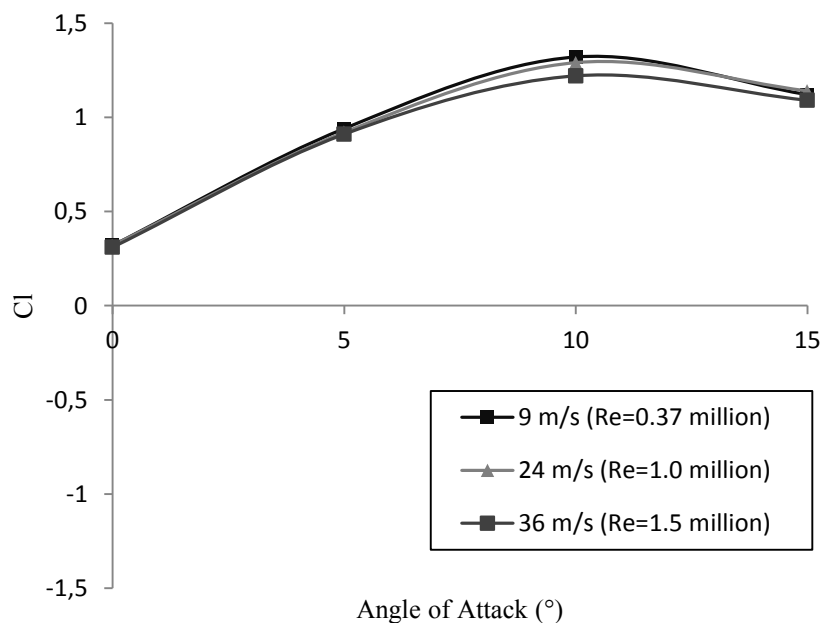
Figure 15. Behavior of S814 for different Reynolds. Source: Janiszewska *et al.* (1996)

Figure 16. Lift coefficient versus the attack angle for different Reynolds number.

Magalhães, G. ; Oliveira, L.A. and Jaouen, P.  
Application of Good CFD Simulation Practices to S814 Airfoil Profile

## 7. CONCLUSION

During the simulations, Cl values were found close to the test values obtained from the wind tunnel. The 40c x 19c domain, in C-mesh shape, is presented as a good practice. Despite the difficulties of generating a structured mesh for complex geometries, better results were presented and the refinement of the mesh near the airfoil contour was fundamental for a good result. It was also confirmed that the Cl value does not vary significantly for different speeds. Thus, this study will provide the basis for performing simulations in other airfoils, as well as simulation of a wind turbine blade in rotation.

## 8. REFERENCES

- Buhl, M., 6 July, 2012. "NWTC Information Portal *NREL*". 13 May, 2013  
<<http://wind.nrel.gov/airfoils/AirfoilFamilies.html>>
- Çengel, Y. A., and Cimbala, J. M., 2007. *Mecânica dos Fluidos - Fundamentos e Aplicações*. McGraw-Hill, São Paulo, 1ª edição.
- Delf University of Technology, 2013. "Low Turbulence Wind Tunnel". 29 April, 2013  
<<http://www.lr.tudelft.nl/en/organisation/departments/aerodynamics-wind-energy-flight-performance-and-propulsion/facilities/low-speed-tunnels/low-turbulence-wind-tunnel/>>
- Edwards, J., and Chandra, S.1996. "Comparison of eddy viscosity-transport turbulence models for three-dimensional, shock separated flowfield". *AIAA journal*, Vol. 34, p. 756-763.
- Germer, E. M. (2009). *Verificação de funções de interpolação em advecção-difusão 1D com volumes finitos*. Dissertação de Mestrado, Curitiba.
- Hansen, M. O. 2008. *Aerodynamics of Wind Turbines*. Earthscan, London, Sterling, VA, EUA, UK: 2<sup>nd</sup> edition
- Hills, J. (2005). *Numerical Modelling of Turbulent Flow past an airfoil*. Czech Technical University, Praga.
- Huang C., Yang K., Liu Q., Zhang L., Bai J., Xu J. 2011. "A study on performance influences of airfoil aerodynamic parameters and evaluation indicators for the roughness sensitivity on wind turbine blade." *Science China Technological Sciences*, Vol. 54, p. 2993-2998.
- Janiszewska, J. M., Ramsay, R. R., M.J.Hoffmann, and G.M.Gregorek. 1996. *Effects of Grit Roughness and Pitch Oscillations on the S814 Airfoil*. Golden, Colorado: National Renewable Energy Laboratory.
- Knoppa, T., Eisfeld, B., and Calvo, J. B. 2009. "A new extension for k- $\omega$  turbulence models to account for wall roughness." *International Journal of Heat and Fluid Flow*, p. 54-65.
- Menter, F. 1993. "Zonal two equation k/x turbulence models for aerodynamic flows." *AIAA Journal*, p. 2906.
- Ribeiro, A.F.P., Awruch A.M., Gomes, H.M. 2011. "An airfoil optimization technique for wind turbines". *Applied Mathematical Modelling*, p. 4898-4907.
- Sagol, E., Reggio, M., & Ilinca, A. 2012." Issues concerning roughness on wind turbine blades." *Renewable and Sustainable Energy Reviews*, p. 514-525.
- SAS IP, I. 2011. ANSYS Manual. *Shear-Stress Transport (SST) k- $\omega$  Model*.
- Schneider, F. A. 2007. *Verificação de soluções numéricas em problemas difusivos e advectivos com malhas não uniformes*. Tese de doutorado, Universidade Federal do Paraná, Setor de Tecnologia, Curitiba.
- Singha, R. K., Ahmeda, M., and Mohammad, Z., Young, L. 2010. "Design of a low Reynolds number airfoil for small horizontal axis wind turbines". *Renewable Energy*, p. 66-76.
- Somers, D. M. 1997. *Design and Experimental Results for the S814 Airfoil*. Golden: National Renewable Energy Laboratory.
- Yuguang, D. S. 2010. "Three dimensional numerical simulations of long-span bridge aerodynamics, using block-iterative coupling and DES." *Computers & Fluids*, p. 1549-1561.

## 9. RESPONSIBILITY NOTICE

The authors are the only responsible for the printed material included in this paper.